

Received April 23, 2019, accepted May 30, 2019, date of publication June 5, 2019, date of current version June 26, 2019.

Digital Object Identifier 10.1109/ACCESS.2019.2920920

# Paper-Based, Hand-Painted Strain Sensor Based on ITO Nanoparticle Channels for Human Motion Monitoring

**DONG-JIN LEE<sup>1</sup> AND DAE YU KIM<sup>1,2</sup>**

<sup>1</sup>Inha Research Institute for Aerospace Medicine, Inha University, Incheon 22212, South Korea

<sup>2</sup>Department of Electrical Engineering, College of Engineering, Inha University, Incheon 22212, South Korea

Corresponding author: Dae Yu Kim (dyukim@inha.ac.kr)

This work was supported in part by the National Research Foundation of Korea (NRF), Ministry of Education through the Basic Science Research Program under Grant 2018R1A6A1A03025523, in part by the National Research Foundation of Korea (NRF) funded by the Ministry of Education under Grant NRF-2019R1A2C1006814, and in part by a Research Grant from Inha University.

**ABSTRACT** Paper-based strain sensors have attracted attention as a cost-effective and environmentally friendly approach to wearable electronic devices. This paper proposes a paper-based strain sensor created solely using hand-painting, which is a simple, equipment-free process utilized in green electronics. Commercial printing paper is coated with polydimethylsiloxane diluted with heptane, which provides moisture resistance and mechanical robustness while increasing the hydrophobicity of the surface. The electrodes and conduction channels are fabricated using a pencil for graphite deposition and a brush for the deposition of tin-doped indium oxide nanoparticles, respectively. With a gauge factor of 41.98 in tensile strain tests and 21.36 in compressive strain tests, our strain sensor exhibits a good sensitivity that is similar to that of previously reported paper-based sensors. We also demonstrate that our proposed strain sensor can be used as a weak motion detection device for humans and robots.

**INDEX TERMS** Paper, strain sensor, motion monitoring, hand-painting process, equipment-free procedure.

## I. INTRODUCTION

In recent years, paper has been recognized as an eco-friendly substrate that provides an inexpensive foundation for the development of transistors [1]–[3], energy storage devices [4]–[6], microfluidic-based biosensors [7], [8], and sensors [9]–[14]. Paper is considered particularly promising for wearable electronics due to its omnipresence, versatility, flexibility, low cost, disposability, and mechanical deformability [15]–[17]. Improvements in paper-handling technology have accelerated the development of simple, versatile paper-based wearable devices [15]. A number of paper-based wearable electronic devices have thus been proposed for use in physical monitoring [18]–[20], physiological sensing [21], actuators [22], and energy storage [23].

Of the many proposed paper-based wearable devices, strain sensors have been widely studied for human motion monitoring, which is an important element for fitness tracking and the prediction of chronic diseases such as osteoporosis [15], [24], [25]. The main operating principle for paper-based strain

The associate editor coordinating the review of this manuscript and approving it for publication was Farid Boussaid.

sensors is the change in the piezoresistance of a conductive material deposited on a paper substrate [26], with mechanical deformation, which is associated with the level of strain on the paper substrate, modifying the conductive material network. Various deposition techniques for the conductive material in paper-based strain sensors have been developed, including inkjet printing [27], solvothermal synthesis [28], vacuum filtration [29], and metal evaporation [30]. Of particular interest are pencil-on-paper methods [17], which are simple, inexpensive, and eco-friendly, utilizing a pencil for the deposition of conductive graphite onto the paper.

We here present an alternative approach for paper-based strain sensors fabricated solely using a hand-painting process. To provide moisture-resistant and mechanically robust properties, the paper is coated with polydimethylsiloxane (PDMS) diluted with heptane, which increases the paper's hydrophobic properties. The contact electrodes are fabricated using a pencil for graphite deposition, while the conduction channels are formed using a brush for the deposition of tin-doped indium oxide nanoparticles (ITO NPs). Graphite and ITO NPs are low-cost and have low cytotoxicity [31], [32]. The entire fabrication process is carried out under ambient

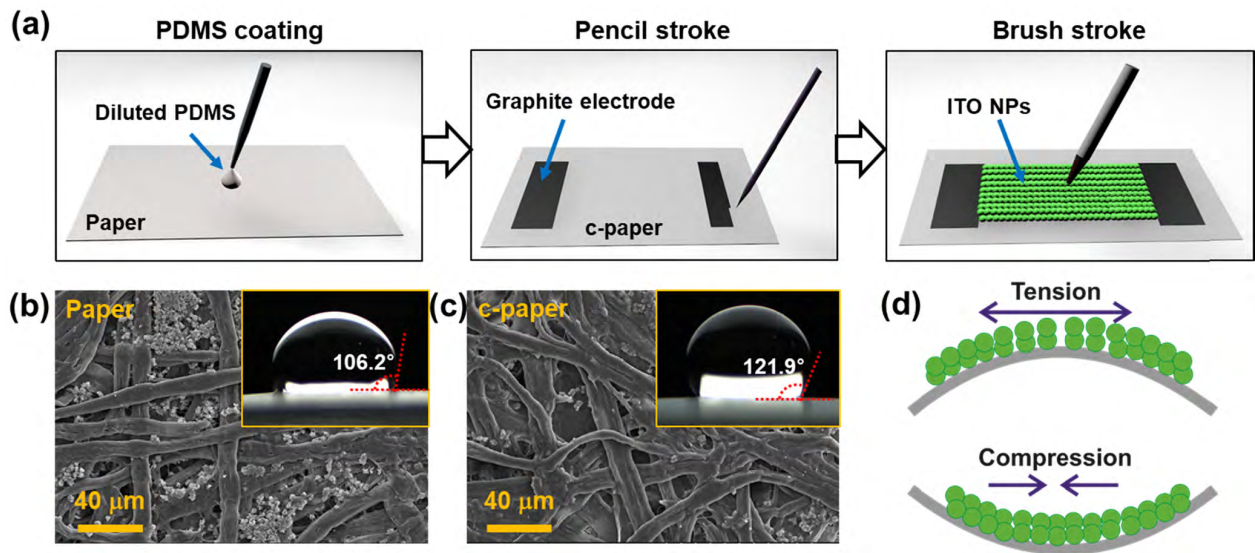


**FIGURE 1.** Schematic diagram and surface properties of the proposed c-paper-based sensor. (a) Schematic illustration of the fabrication process for the c-paper-based strain sensor. Scanning electron microscope (SEM) image of (b) bare paper and (c) c-paper. The insets of (c) and (d) are the representative shapes of water droplets on the bare paper and c-paper substrates, respectively. (d) Sensing mechanism for tensile and compressive strain.

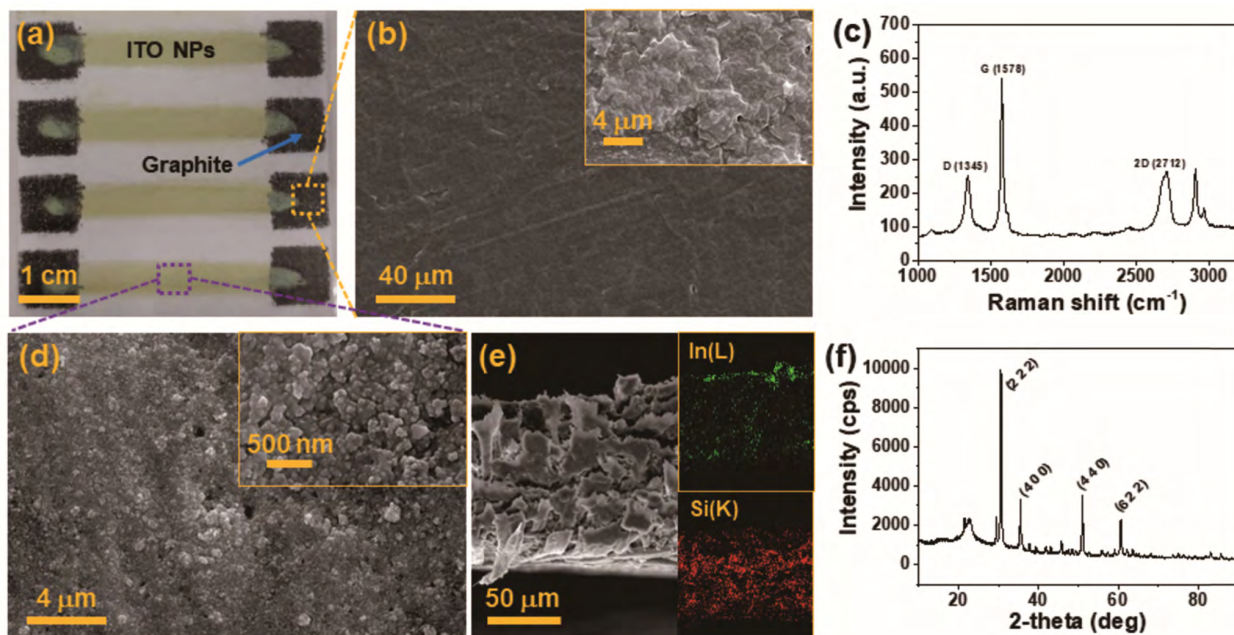


**FIGURE 2.** Morphological and chemical properties of the proposed c-paper strain sensor. (a) Photographic image of a c-paper-based strain sensor. (b) SEM image of a graphite electrode. (c) Raman spectrum of a graphite electrode. The three prominent peaks at 1345, 1578, and 2712 cm<sup>-1</sup> correspond to the D, G, and 2D bands, respectively. (d) SEM image of an ITO NP channel. (e) Cross-sectional SEM image and EDS for an ITO NP channel on the c-paper. (f) XRD spectroscopy of an ITO NP channel. The (222), (400), (440), and (622) planes confirm the crystal structure of the ITO.

conditions and does not require the use of specialized equipment. Our strain sensor exhibits good sensitivity, with a gauge factor of 41.98 in tensile strain testing and 21.36 in compressive strain testing, which is comparable with other sensors based on a paper substrate. We also demonstrate that the fabricated strain sensor has the potential to be used in the real-time monitoring of weak human motion and joint angles in robotics.

## II. EXPERIMENTAL SECTION

### A. MATERIALS

ITO NPs less than 50 nm in diameter were purchased from Sigma-Aldrich Chem. Co., USA. Commercial printing paper was purchased from Double A, Co. Ltd. Polydimethylsiloxane (PDMS, Sylgard 184) was purchased from Dow Corning. Heptane (for HPLC, 99%) was purchased from Sigma-Aldrich.

## B. FABRICATION OF THE PAPER-BASED SENSOR

A schematic of the fabrication process for the proposed paper-based sensor is presented in Fig. 1a. PDMS with a 10:1 ratio of base to cross-linker by mass was diluted with heptane. The diluted PDMS solution (30 wt%) was drop-casted onto the commercial printing paper, and the PDMS-coated paper (c-paper) was cured at room temperature for 48 h. All painting processes were conducted using a plastic mask placed on the c-paper substrate, which had patterns of square electrodes ( $\sim 1 \text{ cm}^2$ ) and a spacing of  $\sim 3 \text{ cm}$  (Fig. S1, Supporting Information). Graphite electrodes were drawn onto the c-paper using a 4B pencil, and a colloidal solution of ITO NPs (10 wt% in ethanol) was deposited on the c-paper using a commercial brush and dried at room temperature. We selected a commercial brush wide enough to cover the width of the pattern with one stroke. To form a stable and dense ITO suspension, the ITO NPs were suspended in 20 mL of ethanol with a concentration of 10 wt%, and the ITO NP suspension was uniformly dispersed using bath sonication for 3 h or more. The entire fabrication process was carried out under ambient conditions and by hand.

## C. CHARACTERIZATION AND MEASUREMENT

The morphology and chemical composition of the paper-based sensor were characterized using scanning electron microscopy (SEM; Hitachi S-4300SE, Hitachi, Tokyo, Japan), energy dispersive X-ray spectroscopy (EDS; Hitachi S-4300SE, Hitachi, Tokyo, Japan), a high-resolution X-ray diffractometer with Cu K $\alpha$  radiation (HR-XRD, X'Pert PRO MRD, Philips, Netherlands), and a Raman spectrometer (HORIBA LabRAM Revolution). The contact angles were characterized using a home-made contact angle measurement system. The sheet resistance of the graphite electrodes and the ITO NP channels were measured using a four-point probe (CMT-SR2000N, AIT, USA).

For strain testing, the ends of the c-paper-based sensor were fixed onto the arms of digital callipers and the bending radius was controlled according to the distance between the two arms. A digital microscope (Celestron LLC, Torrance, CA) connected to a laptop was used to monitor the bending of the strain sensor, and the bending radius was calculated from images captured from the microscope using the MATLAB program (Mathworks Inc., Natick, MA; Fig. S4, Supporting Information). The change in electrical resistance of the c-paper-based strain sensor was monitored with a sourcemeter (Keithley 2400, Tektronix, USA) using two spring clips attached to the ends of the sensor. The applied bias voltage was fixed at 5 V for all experiments.

## III. RESULTS AND DISCUSSION

Figure 1(a) presents a schematic illustration of the fabrication process for the c-paper-based strain sensor. The entire fabrication process was carried out using hand-painting. The network of fibers on the surface of the bare paper and the c-paper was confirmed using SEM images

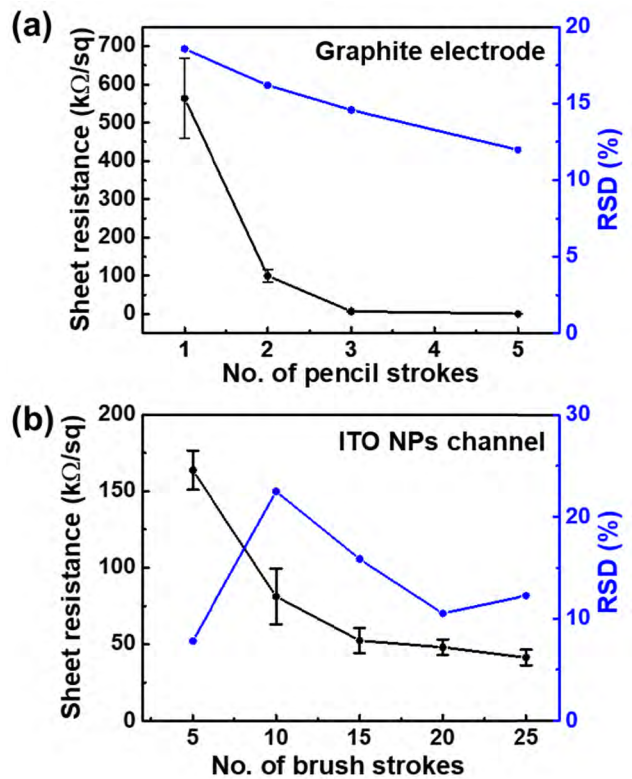


**FIGURE 3.** Sheet resistance (black) and relative standard deviation (blue) of (a) the graphite electrodes with the number of pencil strokes and (b) the ITO NP channels with the number of brush strokes.

(Figs. 1b-c, respectively). The coated film was sufficiently thin, which allowed the fibrous nature of the paper surface to be maintained even after the drop-casting of the diluted PDMS. This contrasts with the approximately 100- $\mu\text{m}$  thick film that formed with the use of a 100 wt% PDMS solution, which leveled the surface and removed the fibrous nature of the paper (Fig. S2, Supporting Information). The contact angles for drops of water on the bare paper and c-paper were  $106.2 \pm 3.8^\circ$  and  $121.9 \pm 4.4^\circ$ , respectively, as shown in the insets of Figs. 1(b)-(c), indicating that the hydrophobicity of the c-paper surface increased compared to that of the bare paper (For more detailed information, see Fig. S3 in Supporting Information). The fabricated c-paper-based strain sensor was fixed onto the arms of digital callipers and the change in resistance was measured for tensile and compressive strain (Fig. 1d).

Cellulose paper has the hygroscopic property of being able to absorb water from the environment. When the relative humidity (RH) increases, the amount of water absorbed on the surface of the cellulose fibers increases, resulting in an increase of ionic conductivity of the paper [41]. The hydrophobic surface modification of the cellulose fibers by diluted PDMS can decrease the hygroscopicity of the fibers, consequently affecting the ionic conductivity of the paper. Thus, the ionic conductivity of the c-paper is lower than that of the untreated paper in a humid environment.

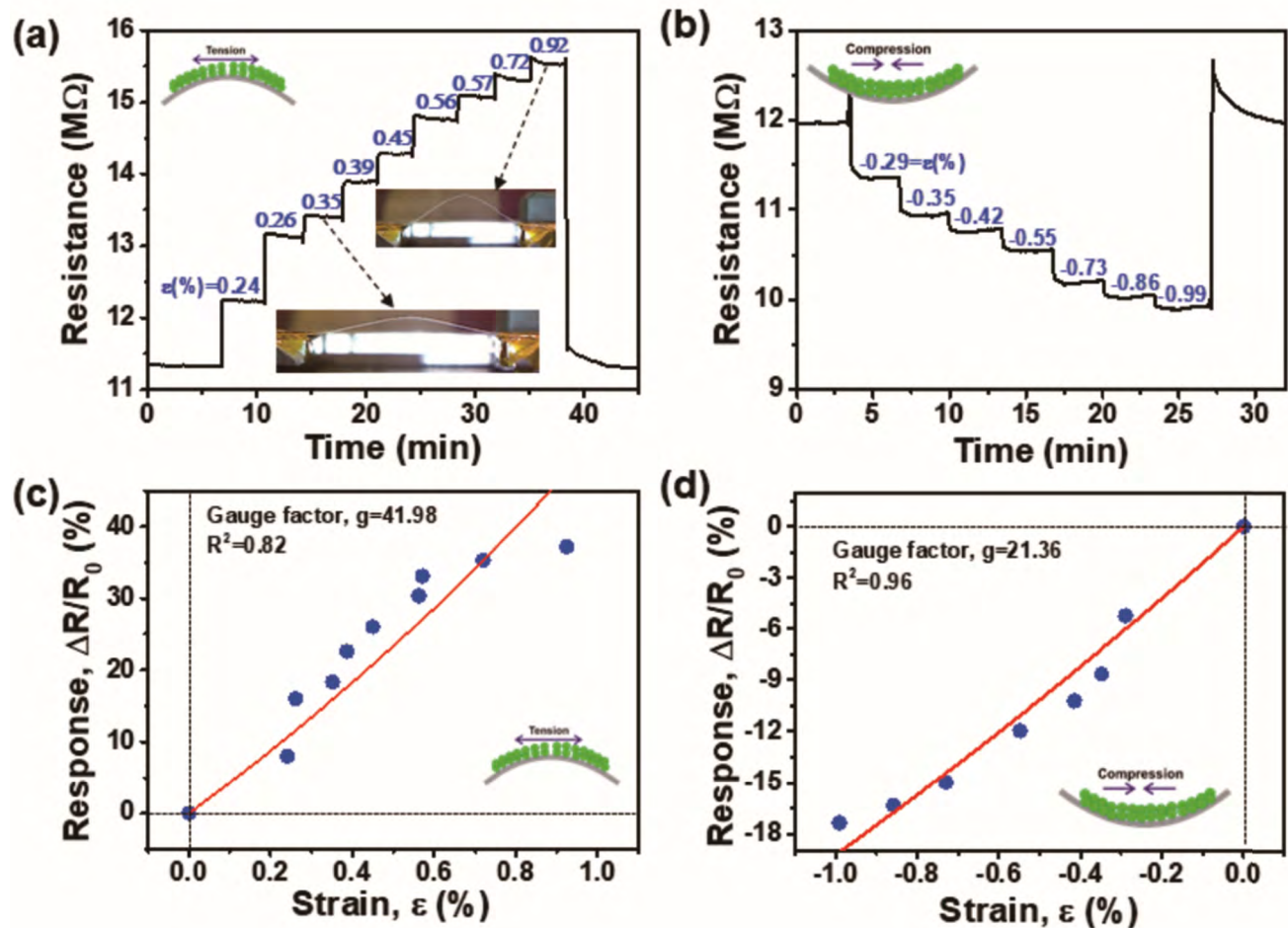


**FIGURE 4.** Sensing properties of the proposed c-paper strain sensor. The real-time sensor response at (a) a tensile strain from 0.24% to 0.92% and (b) a compressive strain from -0.29% to -0.99%. The inset of (a) is the photographic image of the proposed sensor at a tensile strain of  $\epsilon = 0.35\%$  and  $\epsilon = 0.92\%$ . The relative change in resistance versus strain under (c) tensile strain and (d) compressive strain. The gauge factor was derived by fitting the curve to the equation, producing 41.98 for  $R^2 = 0.82$  for tensile strain, and 21.36 for  $R^2 = 0.96$  for compressive strain.

To demonstrate the modification of the hygroscopicity of cellulose paper with hydrophobic treatment, we fabricated a paper-based moisture sensor and monitored the sensor responses in humid air (RH  $\sim 70\%$ ). Figure S11 shows the homemade gas sensor system consisting of a vaporizing gas bottle, a carrier gas (dry air), a mass flow controller (MFC) for each gas line, and a closed chamber. The closed chamber contained a sensor mount and electrical leads. The paper-based moisture sensor was placed on the sensor mount and connected to a Keithley 2400 sourcemeter with a two-probe configuration. The humid air was prepared by blowing dry air (flow rate: 300 sccm) into deionized water in a vaporizing gas bottle, and the RH was calculated using the flow ratio of dry and humid air. The applied bias voltage was at 10 V. LabVIEW software (National Instruments, USA) installed on a laptop computer was used for the sensor measurements and gas monitoring. The paper moisture sensors contained interdigitated Au electrodes (thickness: 200 nm) fabricated using a shadow mask, with a gap of 150  $\mu\text{m}$  between the neighboring electrodes (Fig. S12a). Figure S12(b) shows the temporal

responses of the bare paper and c-paper moisture sensors for humid air with an RH  $\sim 70\%$ . The current increased after exposure to humid air due to the formation of ionic conduction channels along the fibrous network. The sensor response of the c-paper moisture sensor was approximately 4.5 times lower than that of the bare paper moisture sensor, indicating that the amount of water absorbed on the c-paper surface was significantly lower than that on the bare paper. Therefore, the c-paper is capable of providing moisture-resistant properties.

The morphological and chemical properties of the c-paper-based strain sensor are displayed in Fig. 2. Figure 2(a) displays a photographic image of a c-paper-based strain sensor comprising square graphite electrodes and ITO NP channels. An SEM image of the graphite deposited on the c-paper using a pencil is presented in Fig. 2(b). The pencil deposits a diverse range of graphite flakes (inset of Fig. 2b), and the Raman spectrum of the graphite electrode is characterized by a D band ( $\sim 1345 \text{ cm}^{-1}$ ), a G band ( $\sim 1578 \text{ cm}^{-1}$ ), and a 2D band ( $\sim 2712 \text{ cm}^{-1}$ ), as shown

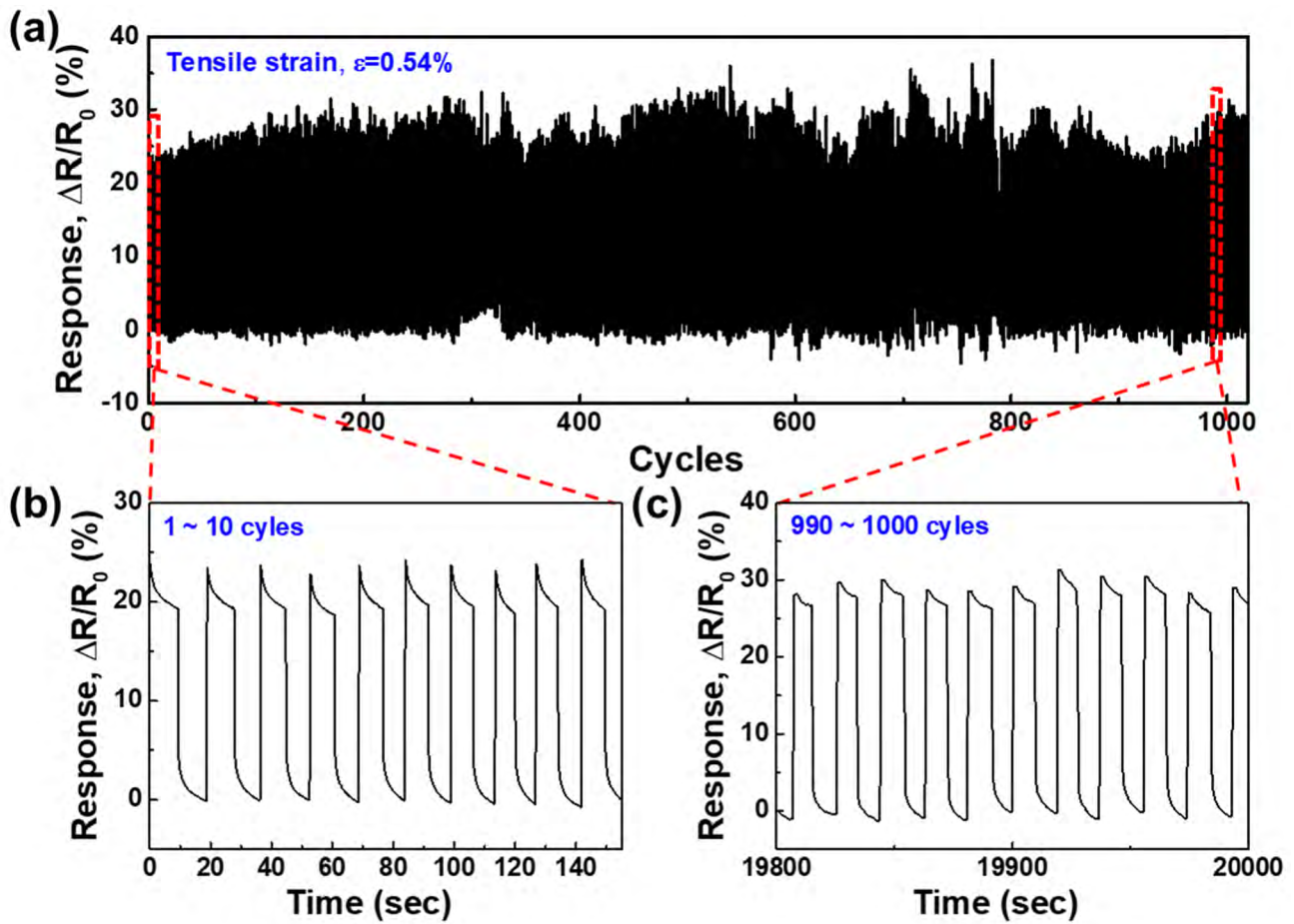


**FIGURE 5.** (a) The sensor response to cyclic loads (> 1000 cycles) for the proposed c-paper strain sensor with a tensile strain of 0.54%. (b) and (c) are the sensor response for 1–10 cycles and 990–1000 cycles, respectively.

in Fig. 2(c). Figure 2(d) presents an SEM image of an ITO NP channel. The painted ITO NPs exhibit a closely packed assembly (inset of Fig. 2d). Figure 2(e) shows a cross-sectional SEM image and energy dispersive X-ray spectroscopy of an ITO NP channel on c-paper. From the observed Si(K) signal originating from the PDMS, it can be seen that the c-paper is entirely coated with PDMS. An In(L) signal was observed on the surface of the c-paper. We also observed XRD peaks due to the (222), (400), (440), and (622) planes, which confirms the crystal structure of the ITO (Fig. 2f).

To ensure uniform electrodes and the ITO NP channels, drawing on the c-paper was conducted with the help of a plastic mask (Fig. S7). As shown in Fig. S7(b), the graphite electrodes and the ITO NP channels had a well-defined shape corresponding to the mask pattern. The number of times the pencil was rubbed on the entire electrode region was named as the number of pencil strokes. Figure 3 shows the variation in the sheet resistance for the graphite electrodes with the number of pencil strokes and for the ITO NP channels with the number of brush strokes. For the graphite electrode, the pencil stroke direction with the number of pencil strokes is shown in Fig. S6. The sheet resistance of the graphite

electrodes exponentially decreased with an increase in the number of pencil strokes (Fig. 3a) due to the decrease in the contact resistance between graphite particles in the percolating network [39]. The mean and relative standard deviation (RSD) for 10 graphite electrodes with 5 pencil strokes were  $0.73 \text{ k}\Omega/\text{sq}$  and 11.98 %, respectively, providing reliable conductive paths [40]. Likewise, the sheet resistance of the ITO NP channels exponentially decreased with an increase of the number of brush strokes (Fig. 3b). The mean and RSD for 14 ITO NP channels with 25 brush strokes were  $41.13 \text{ k}\Omega/\text{sq}$  and 7.52 %, respectively (For more detailed information, See Table S1 in Supporting Information). Based on the above results, we used the graphite electrode with 5 pencil strokes and the ITO NPs channel with 25 brush strokes.

To investigate the uniformity of the ITO NP channels with respect to the stroke direction, we assessed the variation in the sheet resistance based on the stroke direction. Figure S8(a) presents ITO NP channels with 5, 10, 20, and 25 brush strokes. We divided the region of interest with respect to the stroke direction: R1 for the starting region, R2 for the middle region, and R3 for the end region according to the stroke direction. The difference in the sheet resistance on stroke

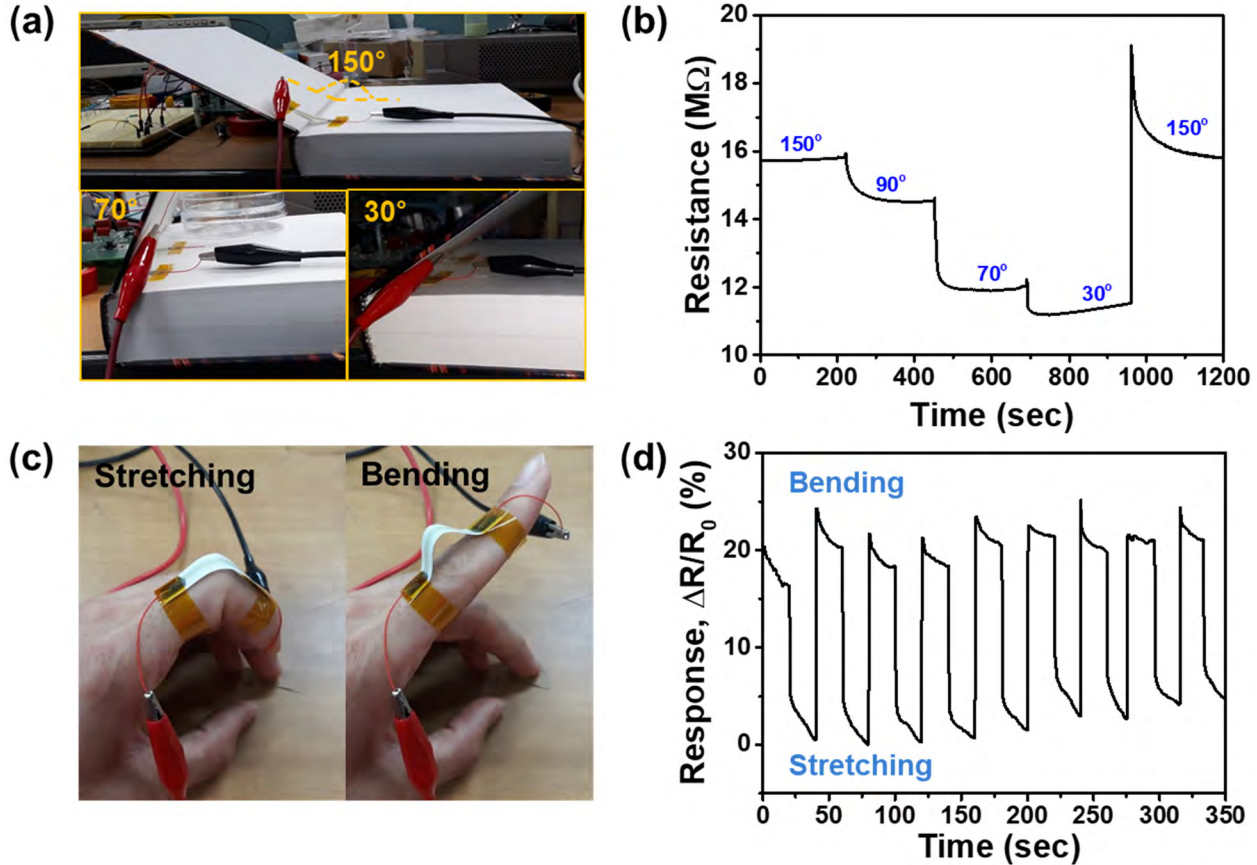


**FIGURE 6.** Monitoring of folding angles and human motion. (a) Photographic images of a c-paper strain sensor fixed in the fold of a book with folding angles of 150°, 70°, and 30°. (b) The change in the resistance of the sensor for decreasing folding angles of 150°, 90°, 70°, and 30°. (c) Photographic images and (d) real-time variation in the relative resistance of the bending and stretching motion of the finger.

direction was below an acceptable level, with an RSD for the ITO NP channels with 5 and 25 strokes of 5.46 % and 7.52 %, respectively (Fig. S8b). These results indicate that the ITO NP channels were uniformly coated on the c-paper using a brush strokes regardless of the stroke direction.

The repeatability of the ITO NP channels was also investigated. We fabricated 10 ITO NP channels with 25 brush strokes and measured the sheet resistance as shown in Fig. S10. The mean and RSD were 42.42 k $\Omega$ /sq and 9.23%, respectively, which was below an acceptable level.

The strain-sensing performance of the proposed sensor was tested using digital callipers to control the bending radius at a strain range from -0.99% (compression) to 0.92% (tension). Figure 4(a)-(b) presents the real-time response at a tensile strain of between 0.24% and 0.92% and a compressive strain of between -0.29% and -0.99%, respectively. The strain  $\varepsilon$  was calculated from the bending radius extracted from the captured images of the c-paper sensor using the equation  $\varepsilon = T/2R_b$ , where  $T$  is the thickness of the c-paper substrate, and  $R_b$  is the bending radius [33], [34]. For our proposed sensor, for a substrate thickness of  $T = 111 \mu\text{m}$ , the change in the bending radius  $R_b$  fell within the range of 6.0 to 23.1 mm for tensile strain and within a range of 5.6 to 19.2 mm

for compressive strain. The resistance increased with tensile strain due to the increase in the interparticle distance and the reduction in electron tunneling. In contrast, for compressive strain, the resistance decreased with an increase in strain.

To investigate the sensitivity of the strain sensor, the relative resistance change on the applied strains was derived by the electron tunneling transport mechanism [34]. The resistance of the conductive nanoparticle arrays were described by quantum tunneling:  $R \propto \exp(\beta d)$ , where  $d$  is the inter-particle distance and  $\beta$  is the electron coupling term. When the inter-particle distance changes from  $d$  to  $d + \Delta d$ , the resistance is changed as following:

$\Delta R \propto \exp(\beta d) [\exp(\beta \Delta d) - 1]$ . Therefore, the relative resistance change is described as following:  $\Delta R/R \propto \exp(\beta \Delta d) - 1 = \exp(g \cdot \varepsilon) - 1$ . By fitting the curve this equation, the gauge factor  $g$  was extracted. As shown in Fig. 4(c)-(d), the extracted gauge factor was 41.98 with  $R^2 = 0.82$  for tensile strain, and 21.36 with  $R^2 = 0.96$  for compressive strain, respectively. The gauge factor is higher for tensile strain than that for compressive strain, due to exponential dependence of relative resistance variation [17]. This gauge factor is higher than that of chrome NP-based and carbon paper-based strain gauges [16], [35].

The main drawback of a thin ITO layer on a flexible substrate under cycle bending is its brittle nature which can lead to significant crack formation, slipping, and delamination after many cycles of compressive and tensile strain [36], [37]. For example, the sputtered ITO layer has a Young's modulus close to 115 GPa, representing a very brittle structure [38]. In contrast, the brittleness of the thin film composed of ITO NPs is less than that of the sputtered ITO layer due to its granular structure [38]. To investigate the brittle nature of ITO NP-based films, their structural stability under cyclic bending was tested. Figure S5 shows the formation of cracks in the ITO NPs channel layer after 100 and 1000 cycles with an applied strain of  $\epsilon = 0.54\%$ . After 100 cycles, minor cracks originating from the defects and impurities on the surface formed (Fig. S5a). However, these cracks did not significantly propagate further after 1000 cycles (Fig. S5b). This is presumably due to the relaxation of stress by early crack formation and the inter-particle adhesive force from van der Waals interactions [33].

To investigate the mechanical robustness and the repeatability of the proposed c-paper sensor, we measured its response to cyclic loads ( $>1000$  cycles) for a tensile strain of 0.54% as shown in Fig. 5. The sensor exhibited a stable response over 1000 cycles with negligible hysteresis.

To study the properties of the c-paper-based strain sensor in response to folding, the sensor was placed in the fold of a book, and the relative resistance was monitored with decreasing folding angles (Fig. 6a). Figure 6(b) presents the real-time variation in resistance as the folding angle decreased from  $150^\circ$  to  $30^\circ$ . The sensor underwent compressive strain as the folding angle decreased, and the sensor resistance progressively decreased. When the sensor returned to its original position, the sensor resistance returned to its initial level. This indicates that the proposed sensor is capable of acting as a foldable sensor for the continuous monitoring of joint angles in robotics. We also investigated the potential of the proposed c-paper-based strain sensor for use in human motion monitoring. The sensor was attached to a finger with Kapton tape as shown in Fig. 6(c). The resistance changed with the bending and stretching of the finger (Fig. 6d). This indicates that the proposed strain sensor could be utilized for the monitoring of weak human motion in wearable devices.

#### IV. CONCLUSION

We proposed and demonstrated a versatile alternative approach to paper-based strain sensors that is fabricated entirely by hand and which requires no special equipment. Our strain sensor demonstrated good sensitivity, with a gauge factor of 41.98 for tensile strain and 21.36 for compressive strain. The c-paper-based sensor was also capable of folding detection over a wide range of angles for the continuous monitoring of joint angles in robotics. In addition, when attached to a finger, our strain sensor successfully monitored bending and stretching motions. We thus believe that the proposed sensor and its fabrication method represent a promising

alternative approach for use in the weak motion monitoring of humans and robots.

#### REFERENCES

- [1] D. Ha, Z. Fang, and N. B. Zhitenev, "Paper in electronic and optoelectronic devices," *Adv. Electron. Mater.*, vol. 4, May 2018, Art. no. 1700593.
- [2] H. Ning, Y. Zeng, Y. Kuang, Z. Zheng, P. Zhou, R. Yao, H. Zhang, W. Bao, G. Chen, Z. Fang, and J. Peng, "Room-temperature fabrication of high-performance amorphous In–Ga–Zn–O/Al<sub>2</sub>O<sub>3</sub> thin-film transistors on ultrasmooth and clear nanopaper," *ACS Appl. Mater. Interfaces*, vol. 9, pp. 27792–27800, Aug. 2017.
- [3] H. Liu, J. Li, and R. Tan, "Flexible In<sub>2</sub>O<sub>3</sub> nanowire transistors on paper substrates," *IEEE J. Electron Devices Soc.*, vol. 5, no. 2, pp. 141–144, Mar. 2017.
- [4] X. N. Zang, C. W. Shen, Y. Chu, B. X. Li, M. S. Wei, and J. W. Zhong, "Laser-induced molybdenum carbide–graphene composites for 3D foldable paper electronics," *Adv. Mater.*, vol. 30, Jun. 2018, Art. no. 1800062.
- [5] A. T. Vicente, A. Araújo, M. J. Mendes, D. Nunes, M. J. Oliveira, O. Sanchez-Sobrado, M. P. Ferreira, H. Águas, E. Fortunato, and R. Martins, "Multifunctional cellulose-paper for light harvesting and smart sensing applications," *J. Mater. Chem. C*, vol. 6, no. 13, pp. 3143–3181, May 2018.
- [6] D. P. Dubal, N. R. Chodankar, D. H. Kim, and P. Gomez-Romero, "Towards flexible solid-state supercapacitors for smart and wearable electronics," *Chem. Soc. Rev.*, vol. 47, pp. 2065–2129, Mar. 2018.
- [7] C. Park, Y. D. Han, H. V. Kim, J. Lee, H. C. Yoon, and S. Park, "Double-sided 3D printing on paper towards mass production of three-dimensional paper-based microfluidic analytical devices (3D-μPADs)," *Lab Chip*, vol. 18, pp. 1533–1538, May 2018.
- [8] N. Alizadeh, A. Salimi, and R. Hallaj, "Mimicking peroxidase activity of Co<sub>2</sub>(OH)<sub>2</sub>CO<sub>3</sub>–CeO<sub>2</sub> nanocomposite for smartphone based detection of tumor marker using paper-based microfluidic immunodevice," *Talanta*, vol. 189, pp. 100–110, Nov. 2018.
- [9] Z. Wang, J. Zhang, L. Liu, X. Wu, H. Kuang, and C. Xu, "A colorimetric paper-based sensor for toltrazuril and its metabolites in feed, chicken, and egg samples," *Food Chem.*, vol. 276, pp. 707–713, Mar. 2019.
- [10] S. Chen, Y. Song, and F. Xu, "Flexible and highly sensitive resistive pressure sensor based on carbonized crepe paper with corrugated structure," *ACS Appl. Mater. Interfaces*, vol. 10, pp. 34646–34654, Sep. 2018.
- [11] X. Qiu and S. Hu, "'Smart' materials based on cellulose: A review of the preparations, properties, and applications," *Materials*, vol. 6, pp. 738–781, Mar. 2013.
- [12] F. Yue, T. S. Ngin, and G. Hailin, "A novel paper pH sensor based on polypyrrole," *Sens. Actuator B, Chem.*, vol. 32, pp. 33–39, Apr. 1996.
- [13] X. Li, Y.-H. Wang, A. Lu, and X. Liu, "Controllable hydrothermal growth of ZnO nanowires on cellulose paper for flexible sensors and electronics," *IEEE Sensors J.*, vol. 15, no. 11, pp. 6100–6107, Nov. 2015.
- [14] A. J. Giménez, G. Luna-Bárcenas, I. C. Sanchez, and J. M. Yáñez-Limón, "Paper-based ZnO oxygen sensor," *IEEE Sensors J.*, vol. 15, no. 2, pp. 1246–1251, Feb. 2015.
- [15] H. Liu, H. Qing, Z. Li, Y. L. Han, M. Lin, H. Yang, A. Li, T. J. Lu, F. Li, and F. Xu, "Paper: A promising material for human-friendly functional wearable electronics," *Mater. Sci. Eng. R, Rep.*, vol. 112, pp. 1–22, Feb. 2017.
- [16] Y. Li, Y. A. Samad, T. Taha, G. Cai, S.-Y. Fu, and K. Liao, "Highly flexible strain sensor from tissue paper for wearable electronics," *ACS Sustain. Chem. Eng.*, vol. 4, pp. 4288–4295, Jun. 2016.
- [17] X. Liao, Q. Liao, X. Yan, Q. Liang, H. Si, M. Li, H. Wu, S. Cao, and Y. Zhang, "Flexible and highly sensitive strain sensors fabricated by pencil drawn for wearable monitor," *Adv. Funct. Mater.*, vol. 25, pp. 2395–2401, Mar. 2015.
- [18] P. Sahatiya and S. Badhulika, "Wireless, smart, human motion monitoring using solution processed fabrication of graphene–MoS<sub>2</sub> transistors on paper," *Adv. Electron. Mater.*, vol. 4, Jun. 2018, Art. no. 1700388.
- [19] G. Ge, W. Huang, J. Shao, and X. Dong, "Recent progress of flexible and wearable strain sensors for human-motion monitoring," *J. Semicond.*, vol. 39, Jan. 2018, Art. no. 011012.
- [20] J. M. Nassar and M. M. Hussain, "Impact of physical deformation on electrical performance of paper-based sensors," *IEEE Trans. Electron Devices*, vol. 64, no. 5, pp. 2022–2029, May 2017.
- [21] M. M. Hamed, A. Ainala, F. Güder, D. C. Christodouleas, M. T. Fernández-Abedul, and G. M. Whitesides, "Integrating electronics and microfluidics on paper," *Adv. Mater.*, vol. 28, no. 25, pp. 5054–5063, Jul. 2016.

- [22] S.-S. Kim, J.-H. Jeon, H.-I. Kim, C. D. Kee, and I.-K. Oh, "High-fidelity bioelectronic muscular actuator based on graphene-mediated and TEMPO-oxidized bacterial cellulose," *Adv. Funct. Mater.*, vol. 25, pp. 3560–3570, Jun. 2015.
- [23] X. Wang, X. Cao, L. Bourgeois, H. Guan, S. Chen, Y. Zhong, D.-M. Tang, H. Li, T. Zhai, L. Li, Y. Bando, and D. Golberg, "N-doped graphene-SnO<sub>2</sub> sandwich paper for high-performance lithium-ion batteries," *Adv. Funct. Mater.*, vol. 22, pp. 2682–2690, Jul. 2012.
- [24] A. Nag, R. B. V. B. Simorangkir, E. Valentin, T. Björnin, L. Ukkonen, R. M. Hashmi, and S. C. Mukhopadhyay, "A transparent strain sensor based on PDMS-embedded conductive fabric for wearable sensing applications," *IEEE Access*, vol. 6, pp. 71020–71027, 2018.
- [25] X. Li, R. Wen, Z. Shen, Z. Wang, K. D. K. Luk, and Y. Hu, "A wearable detector for simultaneous finger joint motion measurement," *IEEE Trans. Biomed. Circuits Syst.*, vol. 12, no. 3, pp. 644–654, Jun. 2018.
- [26] S. K. Mahadeva, K. Walus, and B. Stoeber, "Paper as a platform for sensing applications and other devices: A review," *ACS Appl. Mater. Interfaces*, vol. 7, pp. 8345–8362, Apr. 2015.
- [27] J. Lessing, A. C. Glavan, S. B. Walker, C. Keplinger, J. A. Lewis, and G. M. Whitesides, "Inkjet printing of conductive inks with high lateral resolution on Omnipobic 'R<sup>F</sup>' paper" for paper-based electronics and MEMS," *Adv. Mater.*, vol. 26, pp. 4677–4682, Jul. 2014.
- [28] H. Gullapalli, V. S. M. Vemuru, A. Kumar, A. Botello-Mendez, R. Vajtai, M. Terrones, S. Nagarajaiah, and P. M. Ajayan, "Flexible piezoelectric ZnO-paper nanocomposite strain sensor," *Small*, vol. 6, pp. 1641–1646, Aug. 2010.
- [29] J. Ren, C. Wang, X. Zhang, T. Carey, K. Chen, Y. Yin, and F. Torrisi, "Environmentally-friendly conductive cotton fabric as flexible strain sensor based on hot press reduced graphene oxide," *Carbon*, vol. 111, pp. 622–630, Jan. 2017.
- [30] X. Liao, Z. Zhang, Q. Liang, Q. Liao, and Y. Zheng, "Flexible, cuttable, and self-waterproof bending strain sensors using microcracked gold nanofilms@paper substrate," *ACS Appl. Mater. Interfaces*, vol. 9, pp. 4151–4158, Feb. 2017.
- [31] Y. Tabei, A. Sonoda, Y. Nakajima, V. Biju, Y. Makita, Y. Yoshida, and M. Horie, "In vitro evaluation of the cellular effect of indium tin oxide nanoparticles using the human lung adenocarcinoma A549 cells," *Metalomics*, vol. 7, no. 5, pp. 816–827, 2015.
- [32] Q.-L. Zhao, Z.-L. Zhang, B.-H. Huang, J. Peng, M. Zhang, and D.-W. Pang, "Facile preparation of low cytotoxicity fluorescent carbon nanocrystals by electrooxidation of graphite," *Chem. Commun.*, no. 41, pp. 5116–5118, 2008.
- [33] D. H. Lee, J. Park, J.-K. Lee, K. Heo, D.-J. Lee, Y. R. Lee, and B. Y. Lee, "Highly sensitive and flexible strain sensors based on patterned ITO nanoparticle channels," *Nanotechnology*, vol. 28, no. 49, Dec. 2017, Art. no. 495501.
- [34] J. Yin, P. Hu, J. Luo, L. Wang, M. F. Cohen, and C.-J. Zhong, "Molecularly mediated thin film assembly of nanoparticles on flexible devices: Electrical conductivity versus device strains in different gas/vapor environment," *ACS Nano*, vol. 5, pp. 6516–6526, Aug. 2011.
- [35] M. Zheng, W. Li, M. Xu, N. Xu, P. Chen, M. Han, and B. Xie, "Strain sensors based on chromium nanoparticle arrays," *Nanoscale*, vol. 6, no. 8, pp. 3930–3933, 2014.
- [36] K. Alzoubi, M. M. Hamasha, S. Lu, and B. Sammakia, "Bending fatigue study of sputtered ITO on flexible substrate," *J. Display Technol.*, vol. 7, no. 11, pp. 593–600, Nov. 2011.
- [37] J. Ajuria, I. Ugarte, W. Cambarau, I. Etxebarria, R. Tena-Zaera, and R. Pacios, "Insights on the working principles of flexible and efficient ITO-free organic solar cells based on solution processed Ag nanowire electrodes," *Sol. Energy Mater. Sol. Cells*, vol. 102, pp. 148–152, Jul. 2012.
- [38] T. Königer and H. Münsch, "Coatings of indium tin oxide nanoparticles on various flexible polymer substrates: Influence of surface topography and oscillatory bending on electrical properties," *J. Soc. Inf. Disp.*, vol. 16, no. 4, pp. 559–568, 2008.
- [39] C.-W. Lin, Z. Zhao, J. Kim, and J. Huang, "Pencil drawn strain gauges and chemiresistors on paper," *Sci. Rep.*, vol. 4, Jan. 2014, Art. no. 3812.
- [40] M. P. Down, C. W. Foster, X. Jib, and C. E. Banks, "Pencil drawn paper based supercapacitors," *RSC Adv.*, vol. 6, Jun. 2016, Art. no. 81130.
- [41] F. Güder, A. Ainla, J. Redston, B. Mosadegh, A. Glavan, T. J. Martin, and G. M. Whitesides, "Paper-based electrical respiration sensor," *Angewandte Chemie Int. Ed.*, vol. 55, no. 19, pp. 5727–5732, 2016.

**DONG-JIN LEE** received the Ph.D. degree from the School of Information and Communication Engineering, Inha University, South Korea, in 2016, where he is currently a Research Professor with the Inha Research Institute for Aerospace Medicine. His current research interests include nanoplasmonics and nanoelectronics.



**DAE YU KIM** received the B.S. degree in electrical engineering from Inha University, South Korea, the M.S. degree in electrical engineering from University at Buffalo, The State University of New York (SUNY Buffalo), Buffalo, NY, USA, respectively, and the Ph.D. degree in biomedical engineering from the University of California (UC Davis), Davis, CA, USA, where he was a Med-into-Grad Scholar from the Howard Hughes Medical Institute (HHMI). From 2012 to 2014, he

was a Postdoctoral Scholar with the Biological Imaging Center, Beckman Institute, California Institute of Technology (Caltech), and the Translational Imaging Center, University of Southern California (USC). Since 2017, he has been an Assistant Professor with the Electrical Engineering Department, Inha University, South Korea. His research interests include biomedical optics and imaging to improve diagnosis, treatment, and prevention of human diseases.

• • •